Charger Integrated Coestimation of Parameters and States of Battery

Bikash Sah, *Graduate Student Member, IEEE* and Praveen Kumar, *Senior Member, IEEE*

***Abstract*—Accurate parameter and state estimations of batteries are crucial for increasing safety and reliability. The ageing of batteries leads to electrochemical changes, changing the impedance, and the charge-discharge characteristics. The impedance and derived equivalent circuit model parameters values support state estimation algorithms. Hence, if the parameters of the battery are not updated at regular intervals of time or usage, the state estimation will be erroneous. The battery management system, which performs the state estimation, is limited in functionality and accuracy due to dependency on predefined parameter values fed during the initial set-up. Hence, this work proposes charger-side online parameters and state estimation algorithms based on the impedance and the equivalent circuit parameters determined during the start of charging. The accuracies of the proposed algorithms are verified experimentally for two batteries: A new and an old lithium iron phosphate battery. Further, the algorithms are tested for four types of charging: Constant current, constant current-constant voltage, pulse charging without discharge, and pulse charging with discharge. The experimental results show the suitability of the proposed algorithms for estimating battery parameters and states for both batteries. Moreover, the proposed algorithms are suitable for other Li-ion battery chemistry also.**

***Index Terms*—Capacity, impedance of battery, Li-ion battery, parameter and state estimation, state of charge (SoC).**

I. Introduction

THE demand for transportation electrification worldwide has increased the application of energy storage systems. Li-ion batteries have emerged as the best solution because of high specific power densities, better temperature tolerance, higher constant power range, more usable capacity, and fast charging capabilities. A major challenge to increase the useful lifetime and operational safety of the Li-ion batteries requires accurate determination of parameters and states. The parameters include impedance, total capacity, open circuit voltage (OCV), and equivalent circuit model element values. States include state of charge (SoC), temperature, and real-time capacity [1]. The value of parameters of the battery changes after multiple charge–discharge cycles, while the value of states changes within a charging or discharging process. It is important to note that the value of the parameters and states guide the user to decide the action to charge or stop discharging batteries. Further, overcharging or overdischarging of Li-ion batteries due to inaccurate prediction of its parameter and states leads to fast degradation and safety concerns [2], [3]. Hence, accurate estimation of battery parameters like impedance and state variables, such as SoC and capacity, significantly impact the battery's performance [4].

The impedance of the battery provides valuable information about the degradation, ageing, possible rise in internal temperature, deviation in OCV, and possible safety concerns [3]. An increase in the impedance indicate the electrochemical phenomenon that leads to the increase in the solid electrolyte interface layer thickness, changes in the diffusivity of ions and viscosity of electrolyte, decrease in the porosity, and increase in tortuosity of electrodes [2]. The increasing impedance adds to Joule losses, reducing the charge and discharge efficiency, and increasing self-discharge and the internal rise of battery temperature. Cell venting, fire, or explosions are a few outcomes when heating exceeds safety limits [5]. Further, impedance is an important parameter for estimating other battery states, such as SoC and capacity [6], [7]. Hence, an accurate estimation of the battery impedance will assist in utilization within safety limits.

Since impedance estimation is critical, different methods to estimate impedance are reported in the literature. These are broadly classified into the charge–discharge method, electrochemical impedance spectroscopy (EIS), electrical model, and electrochemical model based. The charge–discharge method does not require complex instruments. However, the estimated value has a visible impact of the measurement noise and the rest period [8], [9]. The use of impedance spectroscopy is widely reported in the literature and has matured over time, resulting in accurate estimation. EIS give complex values of impedance for a wider range of frequencies. The values of impedance at low frequencies are in the range of a few mΩ. Hence, the need for accuracy and precision in measurement makes the equipment costly, especially when the frequency range is from μHz to MHz. Another major drawback of this measurement technique is integrating a separate hardware system that does not support online estimation. Hence, EIS is mostly limited to laboratory applications [10], [11]. Approaches are discussed in the literature to perform online estimation. Broadband impedance spectroscopy, which uses multisine wave excitation and a connected electronic load, is another approach to the online estimation of impedance [12]. The model-based impedance estimation, which utilizes electrical or electrochemical models, has challenges

Manuscript received 22 August 2022; revised 14 November 2022 and 31 January 2023; accepted 3 March 2023. Date of publication 7 March 2023; date of current version 19 May 2023. Recommended for publication by Associate Editor K.-H. Chen. *(Corresponding author: Bikash Sah.)*

The authors are with the Department of Electronics and Electrical Engineering, Indian Institute of Technology Guwahati, Guwahati 781039, India (e-mail: bikash.2015@iitg.ac.in; praveen_kumar@iitg.ac.in).

This article has supplementary material provided by the authors and color versions of one or more figures available at https://doi.org/10.1109/TPEL.2023.3253562.

Digital Object Identifier 10.1109/TPEL.2023.3253562

of complexity and computationally intensiveness, leading to difficulty in realising the method in a microcontroller [13], [14], [15], [16], [17].

Another widely discussed approach is integrating online impedance estimation algorithms in the charger or power-electronics converters connected to batteries. A strategy for such an approach is to attach a calibration device coupled with a power converter, which precisely measures the battery's response to a particular excitation signal. An example of the initial approach is presented in [18], where discrete Fourier transform is used to determine the impedance of a valve regulated lead-acid absorbent glass mat battery. In an another work, the duty cycle of the control signal of a dc–dc converter is perturbed to get sinusoidal current and voltage with dc offset [19]. Since the battery impedance is unknown, the idea of perturbing the duty cycle in [19] suffered from a drawback of the unknown response of voltage and current. The excitation current from the motor controller, along with added electronics are used to perform impedance measurement in [20]. The response of the battery to the excitation current is calibrated, filtered, and using a statistical correlation approach, the information of impedance is extracted.

Koch et al. [21] supplemented the charger with a switched-mode amplifier for generating required current waveforms to perform impedance spectroscopy. The d-q transformation of the injected ac current ripple is also explored to estimate impedance in a high-power charger in [22]. A statistical approach such as the cross-correlation technique integrated into a dc–dc converter is also presented in the literature to determine impedance [23]. Kim et al. [24] presented methodology for state estimation of battery connected to a solar battery charger, where they focused on using the estimation to add protection in the operation. With different algorithms proposed in the literature, sinusoidal excitation and extraction of information from the battery response remain a common approach. The differences are in either hardware used for excitation or the process of information extraction. The impedance information determined from the proposed techniques is used for estimating states such as SoC, OCV, and capacity.

Accurate SoC and capacity estimations of batteries are a challenge to date that researchers are trying to solve using various algorithms. The algorithms are either direct measurement-based, model-based, or hybrid. The simplest and most common direct SoC measurement methods are Coulomb counting, SoC–OCV curve, and lookup table [17]. Model-based estimations are widely used for real-time estimation because of the possibility of updating estimates based on a feedback mechanism [15]. The electrochemical model is based on sets of governing equations and values of parameters that describe the characteristics of a specific battery. Electrical models use properties of voltage and current sources, resistors, and capacitors to model the behavior of batteries. Data-driven models utilize machine learning algorithms such as artificial neural networks, deep neural networks, and support vector machines to model battery properties [25], [26]. These estimations based on the models are supplemented by feedback algorithms such as variants of least square, adaptive observers, Kalman filters, and their combinations [15], [16], [17], [23]. Ampere hour counting, internal resistances based, OCV–SoC curve deviation, and model-based (electrochemical, electrical, and data-driven) are widely proposed techniques for capacity estimation in the literature.

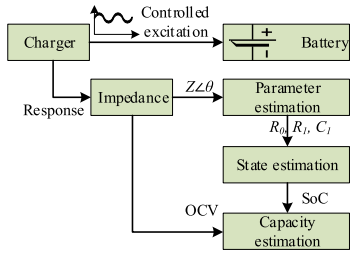

Fig. 1. Schematic representation of the proposed algorithm.

Based on the literature, the major drawbacks of the techniques for determining parameters and states of the batteries are the sensitivity to measurement error, environmental errors, mathematical complexity, and computational cost. Hence, there is a need for less complex estimation algorithms to have an easier implementation with less computation cost. Further, impedance which varies based on the electrochemical phenomenon and ageing in the battery is an important parameter impacting the state estimation accuracy. Hence, impedance and the equivalent circuit model parameters should be estimated before the start of charging. The estimated impedance and the equivalent circuit model parameters can be incorporated in state estimation algorithms to improve the accuracy in the estimation processes irrespective of the ageing of batteries. However, the currently existing impedance measurement techniques have drawbacks such as requirements of a separate hardware system, integration of computationally extensive calibration and estimation algorithms into separate hardware connected with the power converter, and an undetermined amplitude of excitation signals due to changes in the duty cycle of control signals of the power converter.

Taking into consideration all the challenges, requirements, and drawbacks discussed in previous paragraphs, in this work, an algorithm to estimate impedance online and use the impedance values in SoC and capacity estimation is proposed. The contributions of the work are as follows.

1) An online impedance measurement technique for the battery is proposed in this work (Fig. 1) by modifying the reference signal of the dc–dc converter, which performs charging using any type of technique [constant current (CC), constant voltage (CV), CC-CV, and variants of pulse-based charging] and battery electrochemistry. The proposed algorithm in this work circumvents the drawbacks of the existing methods.
2) The impedance estimated online before the start of charging can be extended to estimate online the equivalent circuit model (ECM) parameters of the battery, SoC, and capacity. The process is demonstrated by determining the OCV of the battery using impedance. The SoC estimation is realised using an extended Kalman filter (EKF) based on the ECM parameters determined online. The real-time estimation of impedance and parameters in the EKF makes

the estimation process suitable for all Li-ion batteries, irrespective of age and chemistries.

3) One of the primary focuses of the work is to develop algorithms for parameter and state estimation, which are accurate irrespective of the ageing of the batteries. Since the complexity in the impedance estimation algorithm is reduced and can be incorporated in the charger to estimate impedance and related equivalent circuit parameters, the impact of ageing in state estimation is also incorporated with increased accuracy. The claim is validated by performing parameter and state estimation of an old and a new Lithium-iron phosphate (LFP) battery. Further, the proposal's validity is also checked for a different electrochemistry—Li-graphene battery.
4) The proposed algorithms to estimate the parameter and states of the battery are integrated into the charger along with the charging control algorithm, paving the way for online impedance estimation and eliminating the requirement for additional circuits. The proposed algorithms are verified for their suitability for use in four types of charging techniques viz.: CC, CC-CV, pulse charging without discharge, and pulse charging with discharge on an old and a new battery.

The rest of this article is organized into three sections. Section II describes the algorithms proposed for estimating impedance, SoC, and capacity. Section III presents the results obtained on implementing the algorithms in an experimental setup comprising power electronics converters and a digital signal processer for control and estimation. Finally, Section IV concludes the article with a comprehensive discussion on the outcome of the work.

II. Proposal of Online Parameter Estimation

A. Impedance

The battery's impedance varies with change in SoC, internal or ambient temperature, charge rate (C_{rate}) and discharge rate, ageing, and any change in electrochemistry. The rate of change in impedance is not predictable, making the impedance estimation a challenge. The drawbacks of the works in literature are discussed in the previous section. This work performs the perturbation in the reference signals used in the power converter connecting the battery, as shown in Fig. 1. Since the battery charges using dc inputs, the reference current, and voltage values to charge the battery are constant, a sinusoidal component is added to these constant dc values such that the converter does not go into a discontinuous mode of operation. Since the reference signals are controlled, the output voltage and current at the battery are known and remain under limits.

The controlled dc–dc converter in a charger gives an output of either CC, CV, or pulsed current. The value of load current in CC and pulse charging and the voltage across the battery in CV is decided based on the reference values. Hence, the reference values are updated to get a sinusoidal current and voltage for estimating impedance at the output of the dc–dc converter, which charges the battery. A detailed schematic of the proposed impedance measurement algorithm is given in Fig. 2.

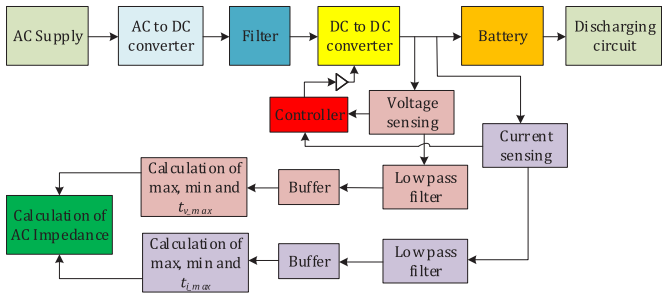

Fig. 2. Schematic representation of the impedance estimation.

Consider a controlled dc–dc converter that is operating to charge using CC charging mode. The reference current $I_o(t)$ is defined as follows:

$$I_o(t) = I_{\text{dc}} + I_{\text{ac}}\sin(2\pi f_p t + \phi_i) \tag{1}$$

where I_{dc} is the dc offset current, I_{ac} is the sinusoid of peak magnitude I_{ac} superimposed over I_{dc}, f_p is the frequency of I_{ac}, and ϕ_i is the phase angle of current. The value of I_{dc} should be less than or equal to $|I_o - I_{\text{ac}}|$. If the converter operates in the CV mode of charging, the variable I can be replaced by V. In response to the reference, the controller of the dc–dc converter will produce the duty cycle as follows:

$$d(t) = D_{\text{dc}} + D_{\text{ac}}\sin(2\pi f_p t + \phi_i) \tag{2}$$

where D_{dc} is the duty cycle for constant offset current, D_{ac} and f_p are the peak magnitude of duty cycle and frequency of waveform to generate $I_o(t)$, respectively. Since the battery has both resistive and capacitive behaviour, the output voltage also follows a sinusoidal pattern with a change in phase angle.

$$V_o(t) = V_{\text{dc}} + V_{\text{ac}}\sin(2\pi f_p t + \phi_v) \tag{3}$$

where V_o is the voltage at the load, V_{dc} is the offset output voltage, V_{ac} is the peak amplitude of sinusoidal voltage output, and ϕ_v is the phase angle of voltage. It is to be noted that all the sinusoids ($I_o(t)$, $d(t)$, and $V_o(t)$) are in the same f_p. For determining the battery's impedance, a cycle of data is stored in the buffer from which the peak to peak values of voltage ($V_{\text{ac}_{pp}}$) and current ($I_{\text{ac}_{pp}}$) are determined. The impedance (Z) of the connected battery is determined by measuring the peak-to-peak values of V_{ac} and I_{ac} and the change in phase angle ($\phi_v - \phi_i$) for a cycle.

$$Z = \frac{V_{\text{ac}_{pp}}}{I_{\text{ac}_{pp}}}\angle(\phi_v - \phi_i). \tag{4}$$

The $\angle(\phi_v - \phi_i)$ can be calculated as $360 \times t_d \times f_p$, where t_d is the difference between $t_{v-\text{max}}$ and $t_{i-\text{max}}$. The $t_{v-\text{max}}$ and $t_{i-\text{max}}$ is the time at which maximum value of voltage and current signals are recorded as shown in (2). The estimated impedance is used to determine the OCV using (5).

$$\text{OCV} = V_{\text{oc}}(\text{SoC}) + I_0 \times Z \tag{5}$$

where $V_{\text{oc}}(\text{SoC})$ is the SoC dependant OCV, and I_0 is the battery current.

Since the work focuses on developing parameter and state estimation algorithms that are accurate irrespective of the ageing

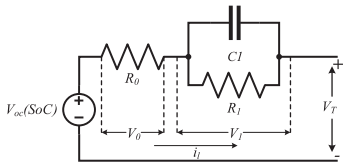

Fig. 3. Electrical equivalent circuit model of the battery.

of the batteries, conventional techniques are used to estimate the SoC of the battery. Further, the capacity is determined using the estimated impedance and OCV using the proposal presented. These are explained in the next subsections.

B. Determination of Equivalent Circuit Parameters

The state estimations in this work are performed using a dynamic electrical model that can capture the characteristics of the battery during charge and discharge. These electrical models comprise mostly the combination of RC components [25]. If the impedance estimated is accurate, the RC components can be determined appropriately to improve the accuracy and increase the application spectrum. Since the impedance and corresponding R and C values are estimated in real-time, the estimated states easily account for the model and measurement uncertainty, thereby complementing the estimation accuracy. The RC model used in this work is relatively simple but captures the dynamics of the battery as described in [22], [25]. The ECM of the battery is shown in Fig. 3. The ECM comprises a resistance in series (R_0) with a single RC network (R_1 and C_1) that captures the response of the battery during transients and a dc source representing the OCV as a function of SoC. The values of these components are required to be computed for implementing any model-based state estimation algorithms. The ECM for a charge current i_l in Fig. 3 is described in (6).

$$\left.\begin{aligned} V_0 &= i_l R_0 \\ \dot{V}_1 &= \tfrac{i_l}{C_1} - \tfrac{V_1}{R_1 C_1} \\ V_T &= V_{\text{oc}}(\text{SoC}) + V_1 + V_0 \\ \text{SoC}_{t+1} &= \text{SoC}_t + \textstyle\int_t^{t+1} \tfrac{\eta \times i_l}{Q} dt \end{aligned}\right\} \tag{6}$$

where V_1 and V_0 are the polarization voltage and the drop across series resistance (R_0), respectively, η is the charge efficiency, and Q is the capacity of the battery. The equations in (6) are used to determine the values of (R_0), (R_1), and (C_1) using recursive least square with variable direction forgetting. Recursive least square (RLS) estimation and its variants viz., weighted RLS, RLS with forgetting factor, and moving window RLS are widely used for parameter identification [28], [29], [30], [31]. This work uses the recursive least square estimation using exponential forgetting (RLSEF) for parameter identification. RLSEF uses the forgetting factor, which decays the droop in the covariance matrix. Further, RLSEF has a faster estimation ability with less prediction error [32]. Since the implementation is to be done online in real-time systems, the (6) is to be converted into the discrete domain. Hence, the required equation is converted to the frequency domain and discretized using the bilinear transformation. The characteristics of the ECM in the frequency domain

Algorithm 1: RLSEF Estimation for Parameter Identification.

1: **Initialize**: $\theta(0)$, $P(0)$, and $\lambda(0)$
2: **Input** $\phi[k]$ based on (15)
3: **Update covariance matrix** using P[k]=$\frac{1}{\lambda}[1 - K[k]\phi^T[k-1]P[k-1]]$
4: **Compute weighing factor** using K[k] = P[k]$\phi[k]$
5: **Prediction error** $\varepsilon[k]$ = y[k] - ϕ^T[k - 1]$\hat{\theta}[k-1]$
6: **Estimation** $\hat{\theta}[k] = \hat{\theta}[k-1]$ + K[k]$\varepsilon[k]$
7: **Identify parameters** using (9)

are expressed in (7).

$$V_T(s) - V_{\text{oc}}(\text{SoC})(s) = i_l(s)\left[R_0 + \frac{R_1}{1 + R_1 C_1 s}\right]. \tag{7}$$

The transfer function [G(s)] of the system is

$$G(s) = \frac{V_L(s)}{i_l(s)} = \left[\frac{R_0 + R_1 + R_0 R_1 C_1 s}{1 + R_1 C_1 s}\right] \tag{8}$$

where V_L is $V_T(s) - V_{\text{oc}}$. The discretization (8) is performed using bilinear transformation $s = \frac{2}{T}\frac{1-z^{-1}}{1+z^{-1}}$ which results in values of R_0, R_1, and C_1 as given in (9).

$$R_0 = \frac{-(a_1 - a_2)}{1 + a_0}, R_1 = \frac{-2(a_0 a_1 + a_2)}{1 - a_0^2}, C_1 = \frac{T(1 + a_0)^2}{4(a_0 a_1 + a_2)} \tag{9}$$

where the variable a_0, a_1, a_2 are given by (10) and the discretized transfer function in simplified form in defined by (11)

$$a_0 = -\frac{T - 2R_1C_1}{T + 2R_1C_1}, a_1 = \frac{R_0T + R_1T + 2R_0R_1C_1}{T + 2R_1C_1},$$
$$a_2 = \frac{R_0T + R_1T - 2R_0R_1C_1}{T + 2R_1C_1} \tag{10}$$

$$G(z^{-1}) = \frac{a_1 + a_2 z^{-1}}{1 - a_0 z^{-1}} \tag{11}$$

where z^{-1} is the unit backward shift operator, and T is the sampling time. Using a_0, a_1, a_2, the (7) is discretized as (12).

$$V_T[k] = V_{\text{oc}}(\text{SoC})[k] + a_0 V_L[k-1] + a_1 i_l[k] + a_2 i_l[k-1]. \tag{12}$$

The parameter identification starts by rearranging (12) into (13)

$$y[k] = \phi^T[k]\theta[k] + \Delta\varepsilon \tag{13}$$

where ϕ^T is the parameter vector, $\theta[k]$ is the regression vector, and $\Delta\varepsilon$ is the effect of input noise in the system. Each vector is characterized in (14) and (15).

$$\theta[k] = [1 \quad V_L[k-1] \quad i_l[k] \quad i_l[k-1]]^T \tag{14}$$

$$\phi[k] = [V_{\text{oc}}(SoC)[k] \quad a_0 \quad a_1 \quad a_2]^T. \tag{15}$$

With the determination of values in (14) and (15), the RLSEF is employed for estimating parameters of ECM. The RLSEF is comprehensively presented in Algorithm 1. $K[k]$ is the adaption gain in the given algorithm.

C. Estimation of the State of Charge

Coulomb counting is the simplest technique requiring measured current to determine SoC. However, the method does not incorporate methods to reduce the noise in the measurement and accumulation of error during estimation. Kalman filter, which uses a solution methodology called sequential probabilistic inference, is the most popular method to estimate SoC. The Kalman filter relies on using a dynamic electrical model (described in the previous subsection) that can capture the characteristics of the battery during charge and discharge.

Linear, extended, unscented, or sigma point and particle filters are different approaches of Kalman filters used to date for estimating SoC. EKF and unscented Kalman filters (UKF) are widely used in literature for estimating SoC. However, EKF is less complex and computationally inexpensive when compared with UKF. Literature has also shown that the precision in estimating states is also not compromised [33], [34]. Further, UKF relies on some unpredictable values to solve the equation to estimate states [33]. Hence, EKF with the values of components of ECM estimated using the algorithm in the previous subsection is used in this work to estimate SoC. EKF relies on the minimum value of the mean square estimate to determine the state, and hence, mitigates the impact of measurement noise and accumulated error.

Based on (6), the state equations in discrete form describing the dynamics are given in (16) and (17).

$$\begin{bmatrix} \text{SOC}_{k+1} \\ V_{1_{k+1}} \end{bmatrix} = \begin{bmatrix} 1 & 0 \\ 0 & e^{\left(-\frac{\Delta t}{R_1 C_1}\right)} \end{bmatrix} \begin{bmatrix} \text{SOC}_k \\ V_{1_k} \end{bmatrix} + \begin{bmatrix} \eta \frac{\Delta t}{C_n} \\ 1 - e^{\left(-\frac{\Delta t}{R_1 C_1}\right)} \end{bmatrix} i_k + w_k \tag{16}$$

$$y_{k+1} = \text{OCV}\left(\text{SOC}_{k+1}\right) + R_o i_k + V_{1_{k+1}} + v_{k+1}. \tag{17}$$

The value of R_0, R_1, and C_1 is taken from Section II-B. The nonlinearities associated with the system are modeled and incorporated as (18) and (19).

$$x_{k+1} = f(x_k, u_k) + w_k \tag{18}$$

$$y_{k+1} = f(x_{k+1}, u_k) + v_{k+1} \tag{19}$$

where $x_k = [\text{SOC}_k V_{fk}]^T$ are the states at time k, u_k is the input current at time k, $f(x_k, u_k)$ symbolizes the dynamic of states at time step k, y_{k+1} is the system measurement at time step $k+1$, and $h(x_{k+1}, u_k)$ represents the measurement model. The EKF estimates the value of states and determines the process using a feedback control mechanism involving steps of time and measurement updates. The current and forward states are determined during the time update, while the measurement update is responsible for improving the posteriori estimate based on the new measurement. An EKF is initialized with a state estimate of $\hat{x}(0)$, error covariance ($P(0)$), process noise covariance (Q), and R as the measurement noise covariance. The estimation of SoC is given in Algorithm 2, where $\hat{x}_{k|k}$ is the posteriori estimate of the state at time step k given measurements up to time step k with a corresponding posteriori covariance $\hat{P}_{k|k}$,

Algorithm 2: EKF Estimation for SoC Estimation.

Input: $\hat{x}(0)$, $P(0)$, Q, R

1: **Prediction steps**

(I) **Priori estimate time update** $\hat{x}_{k+1|k} = F\hat{x}_{k|k} + Bu_k$

(II) **Error covariance time update**

$\hat{P}_{k+1|k} = F\hat{P}_{k|k}F^T + Q_k$

2: **Measurement update steps**

(I) **Kalman gain matrix** $K_{k+1} = \hat{P}_{k+1|k}H_{k+1}^T(S_{k+1})^{-1}$

(II) **Posteriori estimate**

$\hat{x}_{k+1|k+1} = \hat{x}_{k+1|k} + K_{k+1}[y_{k+1} - (h(x_{k+1}, u_{k+1}))]$

(III) **Error covariance measurement update**

$\hat{P}_{k+1|k+1} = (I - K_{k+1}H_{k+1})\hat{P}_{k+1|k}$

$F = \frac{\partial f}{\partial x}|_{\hat{x}_{k|k}, u_k}$ is the linearized state transition matrix, and B is the input matrix applied to the current input, u_k, as in (16). The EKF has been shown to be successful at accurate SOC state estimation, especially when it is fed with the correct covariance magnitudes for the state and measurement noise processes, Q and R. Further, the system model uncertainty with change in the battery is incorporated by the real-time estimation of parameters used in EKF.

D. Capacity

Capacity is estimated using a fuzzy logic estimator (FLE). Unlike other state estimators, FLE does not require mathematical equations describing the system's dynamics. The operation of the FLE is based on a set of rules defined by the developer using the knowledge base. The rules are framed to capture the nonlinearity of a system. Further, studies have shown an increase in the accuracy of an FLE when an appropriate shape and number of membership functions are selected [35], [36]. In this work, the inputs to FLE are SoC estimated using EKF, and the OCV is computed based on the impedance of the battery.

Mamdani and Sugeno are the two types of fuzzy logic systems widely discussed in the literature. Of the two, in this work, the Mamdani type FLE is used to determine capacity because of the possibility of defining the rule base based on the developer's intuitive nature and the property of interpretability. The rules are defined using triangular membership functions (MFs) because of the simplicity in implementation, less computational cost, and ability to yield optimal outputs. The choice of the number of MFs is a tradeoff between the accuracy and complexity of the system. A higher number of MFs can improve the accuracy of the system, but it also increases the complexity of the computation. For example, a large number of MFs can lead to overfitting and poor generalization, while a smaller number of MFs can lead to underfitting and poor performance. It's important to carefully evaluate the tradeoffs and choose the number of MFs that best suit the specific requirements of the system [38], [39]. Expert knowledge-based, empirical, analytical, and heuristics are a few approaches mentioned in the literature to determine the number of MFs. Of the different approaches to deciding the number of MFs, a knowledge-based and empirical approach is considered in this work. Fig. 4 shows the structure of the FLE. Consider a

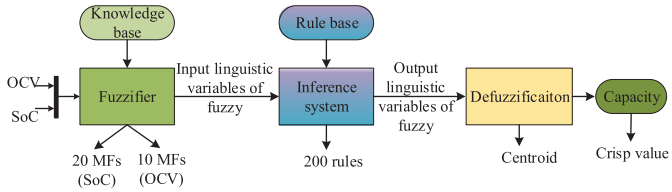

Fig. 4. Schematic representation of the capacity estimation.

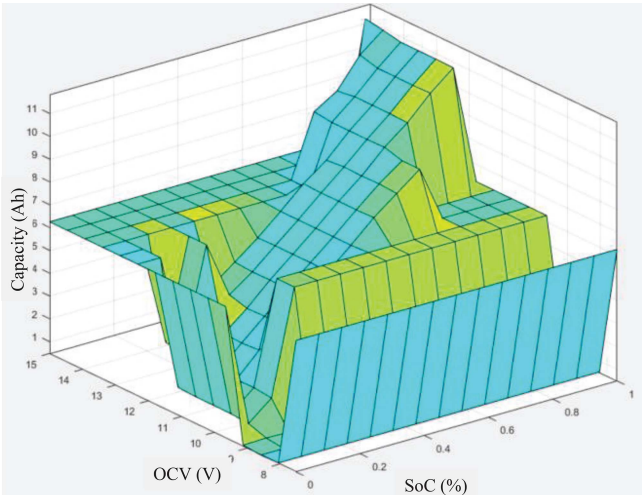

Fig. 5. Surface plot of the rules in the inference system of the FLE.

triangular MF defined in $\Re$ in a range $[a, c]$, with a mid value of b, slope of σ, the fuzzification of the input value x is defined by (20).

$$(x) = \begin{cases} 0, x \in]-\infty,\ a] \ \cup \ [c, \infty] \\ \frac{x-a}{b-a} if\ x \in [a, b] \\ \frac{x-c}{b-c} if\ x \in [b, c]. \end{cases} \tag{20}$$

The OCV inputs are fuzzified using 10 MFs symmetrically distributed ranging from 7.5 to 15 V, the SoC using 20 MFs symmetrically distributed ranging from 0 to 1 (0 % to 100 %), and the capacity using 20 MFs symmetrically distributed ranging from 0 to 12.5 Ah. The fuzzified inputs are passed to the inference system, which is based on max–min inference and has rule base developed based on the knowledge and experience of the expected outputs. The inference system is supported by the rule base designed by developers, And, Or, implication, and aggregation processes. The surface plot of the rules is shown in Fig. 5. The centroid method (21) is used for the defuzzification process. The output of the defuzzification process of FLE is the crisp value (capacity).

$$x_* = \frac{\int \mu_c(x).xdx}{\int \mu_c}(x)dx \tag{21}$$

where x is the input fuzzified in considering the range of MFs, $x_\star$ is the value of centroid (defuzzified output), and $\int$ denotes an algebraic integration.

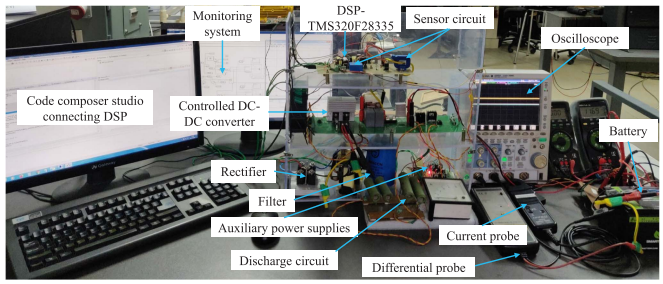

Fig. 6. Experimental setup developed to validate all the algorithms.

III. Experimental Validation

An experimental setup is developed to validate and check the effectiveness of the proposed battery parameter and state estimation algorithms. Hardware-in-loop testing is a simplistic and fast approach to testing the proposed algorithm in a practical system. The experimental setup developed to test algorithms is shown in Fig. 6. The setup comprises a Crydom rectifier module-M5060TB1000 with output *LC* filter, a dc–dc converter (buck topology), a controlled discharge circuit comprising resistive load, and Heliocentris programmable electronic load (EL2400), LEM LV25-P, and LEM HO 50-S as voltage and current transducers, respectively. The specifications of the power converter and electronic load are given in Table S.1. TMS320F28335, a 32-bit microcontroller with 12-bit, 12.5 M samples/second analog-to-digital converters (ADCs), is used to realize the close loop digital controller.

The monitoring desktop is configured to perform a real-time simulation of the estimation algorithms, including impedance, SoC, and battery capacity. The proposed algorithm is verified in a new and an old battery based on the availability in the laboratory. The batteries are of LFP electrochemistry. Both batteries are rated at 12.8 V nominal voltage and 12 Ah capacity. The details of the batteries are given in Table. S.2. Apart from the mentioned details of the experimental setup, YOKOGAWA 700924 differential voltage probe and HAMEG HZ050 current probe are used to record appropriate current and voltage waveforms using the YOKOGAWA DLM2054 oscilloscope.

An overview of the algorithms implemented in the experimental setup is shown in Fig. S.1. The figure comprehensively presents all the algorithms and shows the utilization of the estimated impedance and related parameters of ECM. The state estimation starts after the parameter estimation is complete. The parameter estimation algorithm is expected to be initiated every time before the start of charging. The parameters required for the state will be updated, increasing estimation accuracy. Further, the decrease in the accuracy of the estimation algorithms due to the ageing of batteries is also mitigated.

1) Impedance Estimation: The estimated impedance is based on the process described in Section II-A at $f_p = 1$ kHz. The suitability of f_p is determined based on the test frequency mentioned in the battery datasheets from different manufacturers [37], [38], [39]. Examples of real-time impedance estimation of the old and

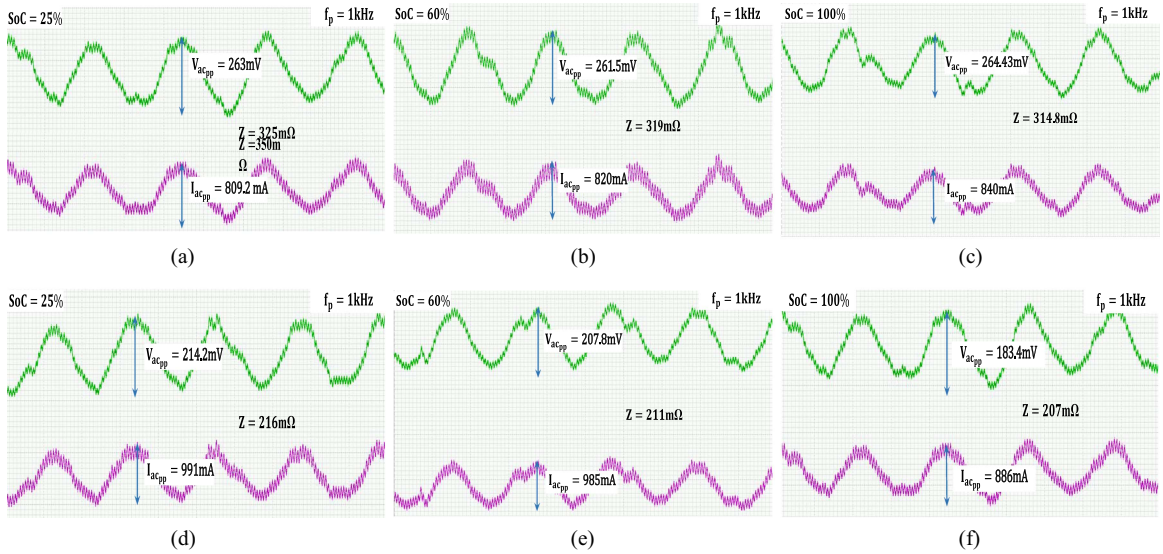

Fig. 7. Determined values of impedances online at different SoC values for the two batteries. (a) Old battery- SoC 25%. (b) Old battery- SoC 60%. (c) Old battery- SoC 100%. (d) New battery- SoC 25%. (e) New battery- SoC 60%. (f) New battery- SoC 100%.

TABLE I
ECM PARAMETERS OF THE BATTERY DETERMINED FROM TEST

ECM parameters of battery			
Parameters	R0 (Ω)	R1 (Ω)	C1 (F)
Old	0.358	0.17	35890
New	0.19	0.05	26560

the new battery variants are shown in Fig. 7. The impedance is used to determine the OCV and capacity. The parameters of the battery are identified online using RLSEF (Section II-B) is given in Table I. The estimated values show that higher ageing has a high value of impedance when compared to the new battery. Further, the resistance (R_0) of the old battery is approximately four to five times higher in comparison with a new battery.

A. Parameter Identification of the Batteries

1) OCV–SoC Test: The accurate estimation of the SoC requires the determination of OCV. The OCV is estimated using (5). Further, OCV is a parameter which varies based on the changes in the equilibrium potential of the battery. Hence, true OCV is determined either by allowing the battery to rest for an extended period such that the change in OCV is lower than 1 mV/min, or a very low (C/20) charging and discharging rate is used [23]. A very low charging and discharging rate allow the battery to remain close to electrochemical equilibrium. Using the relaxation time method is challenging, time consuming, and has possible errors due to unknown relaxation times of battery. Hence, C/20 is charging, and discharging method is used. The setup shown in Fig. 6 is used to perform the test. The curves of OCV versus SoC obtained using the experiment for the two batteries are shown in Fig. S.2 and the coefficients of curve fit are given in Table S.3.

2) SoC and Capacity Estimation: SoC in this work is estimated using EKF based on the online ECM parameters estimated and the OCV–SoC curve. The working of the EKF is described in the previous section. The OCV–SoC curve is used to determine a relationship in the form of a higher-order polynomial equation. Although the work is focused on determining SoC during charging, both charging and discharging are done to record the effect of hysteresis in the battery due to ageing. The discharge test starts after inspecting the terminal voltage is 14.6 V, which infers the full charge state of the battery. Since, at a lower charge and discharge rate, the terminal voltage is equal to OCV, a constant discharge of C/20 is performed, monitoring the terminal voltage of the battery. On reaching 8 V, the cut-off voltage of the battery, the batteries are discharged at a constant voltage to reduce the discharge current to C/50. After complete discharge, the batteries are charged at a C/20 rate up to 14.6 V. On reaching 14.6 V, the CV mode is activated until the charge current reduces to C/50. The monitoring of the terminal voltage leads to the OCV values, and the current help to determine the SoC using the coulomb counting (CC) method (22).

$$\mathrm{SOC}_k = \mathrm{SOC}_0 - \int_{k_0}^{k} \eta_c I_L(\tau) d\tau / C_{\mathrm{nominal},k} \qquad (22)$$

where SOC_0 is the initial SoC of the battery, η_c is the charge or discharge efficiency, $I_L(\tau)$ is the charge or discharge current at time τ, and $C_{\mathrm{nominal},k}$ is the nominal capacity. While performing the charge-discharge test, since the terminal voltage is either maximum or minimum, the SOC_0 is taken as 100% or 0%, respectively. The SoC determined using CC is used as a reference while validating the estimated SoC using EKF. The OCV–SoC curve is shown in Figs. S.2a and S.2b. The difference between the charging and discharging voltage for the old battery is more signifying the increase in the hysteresis with the ageing of the battery. A ninth-order polynomial fit is performed to use in the SoC estimation of battery using EKF. The coefficients are given in Table S.3. The next subsection will present a robustness study

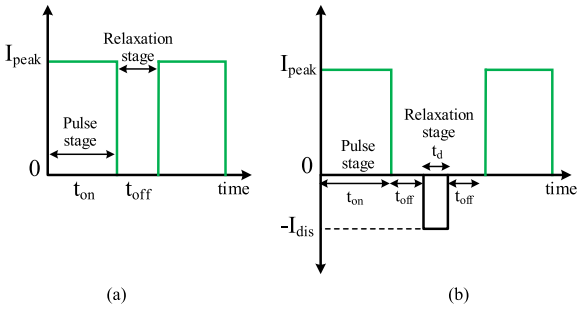

Fig. 8. Waveforms of variants of pulse charging: (a) PCWD and (b) PCWiD.

in estimation based on the estimated parameters during different charging techniques.

The estimated SoC and OCV are used to determine the capacity further using FLE. Since SoC and OCV are translated into 10 and 20 MFs, respectively, 200 rules are formulated in the rule base supporting the inference system. The capacity used for comparison is determined using the current and time data logged using the OCV–SoC test. The algorithms were also tested for a new battery of different electrochemistry— Li-graphene, whose results are presented in supplementary file (S.1.A.).

B. Validation of Proposed Algorithms for Different Charging Techniques

The estimation of impedance, SoC, and capacity is validated for four different types of charging algorithms, viz., CC, constant current constant voltage pulse charging without discharge (PCWD), and pulse charging with discharge (PCWiD). The experiments are performed at three different charging currents of 2, 3, and 4 A. In the case of PCWD and PCWiD (Fig. 8), the average charging current is maintained at respective current defined (2, 3, and 4 A). A period of 60 s is fixed for PCWD and PCWiD. The values of peak amplitude of current (I_{peak}), off time (t_{off}), on time (t_{on}), rest period (t_{off} in PCWD and $2t_{\text{off}} + t_d$ in PCWiD), and discharge pulse period is determined based on (23) and (24).

$$I_{\text{avg}} = \frac{t_{\text{on}}}{t_{\text{on}} + t_{\text{off}}} \times I_{\text{peak}} \tag{23}$$

$$I_{\text{avg}} = \frac{1}{t_{\text{on}} + 2t_{\text{off}} + t_d} \times \left[(t_{\text{on}} \times I_{\text{peak}}) - (t_d \times I_{\text{dis}})\right]. \tag{24}$$

With an increase in rest periods, the peak amplitude increases to maintain the same average current. Further, the addition of a discharge pulse adds to an increase in the peak amplitude. In this work, the time period of a pulse for both PCWD and PCWiD is kept at 60 s. Hence, as an example, for PCWD, to maintain an average current of 2 A, the I_{peak} is 2.5 A for $t_{\text{on}} = 48$ s and $t_{\text{off}} = 12$ s. Similarly, for PCWiD, for maintaining an average current of 2 A, the I_{peak} is 3.142 for $t_{\text{on}} = 48$ s and $t_{\text{off}} = 6$ s and $t_d = 6$ s. The estimated SoC and capacity for different charging current, for four different charging techniques are given as a supplementary material in Figs. S.3 and S.4. Further, to distinguish the estimation results and compute errors, plots with zoomed version are also provided in Figs. S.5 and S.6.

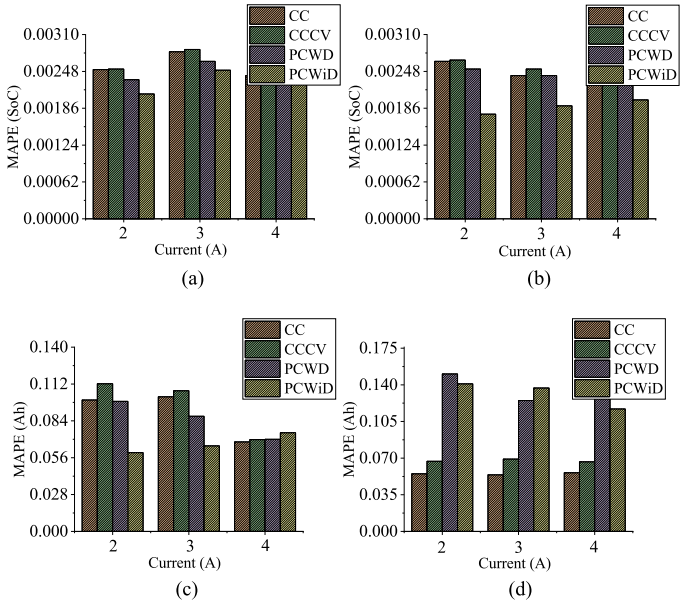

Fig. 9. Errors in SoC and capacity estimation of new and old battery for different charging techniques.

In the plots, the real SoC and capacity are the values computed while determining OCV–SoC curves. The plots of SoC and capacity follow the real values for each charging technique. Further, the robustness of the estimation algorithm is determined in the next subsection.

C. Robustness Study Against Variation of Charging Techniques

The work in literature performs a robustness study by varying the values of impedances and adding artificial noise in the inputs to the algorithm. This work performs the estimation in a real-time system with actual sensor noise. Further, to verify the robustness with ageing, an aged battery which has degraded by approximately 25% to its full capacity is considered. The mean average percentage error (MAPE) between actual values and the estimated is calculated as a robustness parameter. The estimation error in SoC and capacity are shown in Fig. 9 and the MAPE of each are plotted in Fig. 9(a) and (b), respectively. The estimation error in SoC and capacity is least when the CC technique is used. The error in CCCV is comparable to CC because a major part of the charging is dominated by CC. The discharge period in PCWiD keep the rise in the terminal voltage of the battery closer to the value of OCV–SoC curve determined. Hence, in most of the cases, PCWiD shows least error in both SoC and capacity estimation. However, low value of estimation errors for different charging types, charging current, and ageing of battery, validates the robustness of the proposed algorithms.

IV. Conclusion

This work presents a proposal to estimate the batteries' real-time parameters and states. Impedance and the ECM parameters are required when in model-based state estimation algorithms.

An impedance estimation technique is proposed that is implementable without adding any extra circuitry or formulating a complex algorithm. The existing power electronics circuit, which charges the battery, can generate required signals by modifying the reference signal. Capacity degradation or ageing is seen in the batteries due to electrochemical changes. The degradation is reflected as an increase in impedance. The increase in impedance impacts the values of the electrical equivalent circuit parameters, which are used to estimate the states such as SoC and capacity. The accuracy of the states estimation algorithm further depends on the robustness of the selected algorithm for estimation and the make of the cell. Hence, a real-time determination of impedance and related parameters adds accuracy in estimating the associated states such as SoC and capacity. The accuracies of the proposed algorithms are validated in an experimental setup by implementing different charging types, viz., CC, CC-CV, pulse charging without discharge, and pulse charging with discharge. Further, two types of LFP batteries—new and aged—are used to validate the proposal to estimate accurately irrespective of a significant change in impedance due to ageing. The accuracy of the proposed online estimation algorithm proves the competency and ability to reduce the impact of ageing. Additionally, the work opens directions for research in chargers with integrated parameter and state estimations. The integration will help to develop online condition monitoring models, which can provide suggestions to limit the rate of charge and discharge and increase the safety of battery packs.

Supplementary Data and Information: The relevant data supporting the proposal and results are attached in continuation to this manuscript.

REFERENCES

[1] X. Lin and A. G. Stefanopoulou, "Analytic bound on accuracy of battery state and parameter estimation," *J. Electrochem. Soc.*, vol. 162, no. 9, Jul. 2015, Art. no. A1879. [Online]. Available: https://dx.doi.org/10.1149/2.0791509jes

[2] J. Vetter et al., "Ageing mechanisms in lithium-ion batteries," *J. Power Sources*, vol. 147, no. 1-2, pp. 269–281, 2005.

[3] T. Osaka, S. Nakade, M. Rajamäki, and T. Momma, "Influence of capacity fading on commercial lithium-ion battery impedance," *J. Power Sources*, vol. 119, pp. 929–933, 2003.

[4] Y. Wang et al., "A comprehensive review of battery modeling and state estimation approaches for advanced battery management systems," *Renewable Sustain. Energy Rev.*, vol. 131, 2020, Art. no. 110015.

[5] S. Pelletier, O. Jabali, G. Laporte, and M. Veneroni, "Battery degradation and behaviour for electric vehicles: Review and numerical analyses of several models," *Transp. Res. Part B: Methodological*, vol. 103, pp. 158–187, 2017.

[6] J. Sihvo, T. Roinila, T. Messo, and D.-I. Stroe, "Novel online fitting algorithm for impedance-based state estimation of li-ion batteries," in *Proc. 45th Annu. Conf. IEEE Ind. Electron. Soc.*, 2019, vol. 1, pp. 4531–4536.

[7] C. Fleischer, W. Waag, H.-M. Heyn, and D. U. Sauer, "On-line adaptive battery impedance parameter and state estimation considering physical principles in reduced order equivalent circuit battery models: Part 1. requirements, critical review of methods and modeling," *J. Power Sources*, vol. 260, pp. 276–291, 2014.

[8] C. Zhang, J. Liu, and S. Sharkh, "Identification of dynamic model parameters for lithium-ion batteries used in hybrid electric vehicles," 1970.

[9] K. Onda, M. Nakayama, K. Fukuda, K. Wakahara, and T. Araki, "Cell impedance measurement by laplace transformation of charge or discharge current–voltage," *J. Electrochem. Soc.*, vol. 153, no. 6, 2006, Art. no. A1012.

[10] P. A. Lindahl, M. A. Cornachione, and S. R. Shaw, "A time-domain least squares approach to electrochemical impedance spectroscopy," *IEEE Trans. Instrum. Meas.*, vol. 61, no. 12, pp. 3303–3311, Dec. 2012.

[11] J. Christophersen, J. Morrison, W. Morrison, and C. Motloch, "Rapid impedance spectrum measurements for state-of-health assessment of energy storage devices," *SAE Int. J. Passenger Cars - Electron. Elect. Syst.*, vol. 5, no. 1, pp. 246–256, 2012.

[12] A. Waligo and P. Barendse, "A comparison of the different broadband impedance measurement techniques for lithium-ion batteries," in *Proc. IEEE Energy Convers. Congr. Expo.*, 2016, pp. 1–7.

[13] G. K. Prasad and C. D. Rahn, "Model based identification of aging parameters in lithium ion batteries," *J. Power Sources*, vol. 232, pp. 79–85, 2013.

[14] A. P. Schmidt, M. Bitzer, Á. W. Imre, and L. Guzzella, "Model-based distinction and quantification of capacity loss and rate capability fade in li-ion batteries," *J. Power Sources*, vol. 195, no. 22, pp. 7634–7638, 2010.

[15] G. S. Misyris, D. I. Doukas, T. A. Papadopoulos, D. P. Labridis, and V. G. Agelidis, "State-of-charge estimation for li-ion batteries: A more accurate hybrid approach," *IEEE Trans. Energy Convers.*, vol. 34, no. 1, pp. 109–119, Jan. 2018.

[16] G. Sethia, S. K. Nayak, and S. Majhi, "An approach to estimate lithium-ion battery state of charge based on adaptive lyapunov super twisting observer," *IEEE Trans. Circuits Syst. I: Regular Papers*, vol. 68, no. 3, pp. 1319–1329, Mar. 2020.

[17] L. Lu, X. Han, J. Li, J. Hua, and M. Ouyang, "A review on the key issues for lithium-ion battery management in electric vehicles," *J. Power Sources*, vol. 226, pp. 272–288, 2013.

[18] D. Depernet, O. Ba, and A. Berthon, "Online impedance spectroscopy of lead acid batteries for storage management of a standalone power plant," *J. Power Sources*, vol. 219, pp. 65–74, 2012. [Online]. Available: https://www.sciencedirect.com/science/article/pii/S0378775312011780

[19] W. Huang and J. A. Abu Qahouq, "An online battery impedance measurement method using DC-DC power converter control," *IEEE Trans. Ind. Electron.*, vol. 61, no. 11, pp. 5987–5995, Nov. 2014.

[20] D. A. Howey, P. D. Mitcheson, V. Yufit, G. J. Offer, and N. P. Brandon, "Online measurement of battery impedance using motor controller excitation," *IEEE Trans. Veh. Technol.*, vol. 63, no. 6, pp. 2557–2566, Jun. 2014.

[21] R. Koch, R. Kuhn, I. Zilberman, and A. Jossen, "Electrochemical impedance spectroscopy for online battery monitoring - Power electronics control," in *Proc. 16th Eur. Conf. Power Electron. Appl.*, 2014, pp. 1–10.

[22] Y.-D. Lee, S.-Y. Park, and S.-B. Han, "Online embedded impedance measurement using high-power battery charger," *IEEE Trans. Ind. Appl.*, vol. 51, no. 1, pp. 498–508, Jan. 2015.

[23] T. N. Gücin and L. Ovacik, "Online impedance measurement of batteries using the cross-correlation technique," *IEEE Trans. Power Electron.*, vol. 35, no. 4, pp. 4365–4375, Apr. 2019.

[24] I.-S. Kim, P.-S. Ji, U.-D. Han, C.-G. Lhee, and H.-G. Kim, "State estimator design for solar battery charger," in *Proc. IEEE Int. Conf. Ind. Technol.*, 2009, pp. 1–6.

[25] T. Ouyang, P. Xu, J. Lu, X. Hu, B. Liu, and N. Chen, "Co-estimation of state-of-charge and state-of-health for power batteries based on multi-thread dynamic optimization method," *IEEE Trans. Ind. Electron.*, vol. 69, no. 2, pp. 1157–1166, Feb. 2022.

[26] E. Chemali, P. J. Kollmeyer, M. Preindl, and A. Emadi, "State-of-charge estimation of li-ion batteries using deep neural networks: A machine learning approach," *J. Power Sources*, vol. 400, pp. 242–255, 2018. [Online]. Available: https://www.sciencedirect.com/science/article/pii/S0378775318307080

[27] Y. Xing, W. He, M. Pecht, and K. L. Tsui, "State of charge estimation of lithium-ion batteries using the open-circuit voltage at various ambient temperatures," *Appl. Energy*, vol. 113, pp. 106–115, 2014.

[28] M. Verbrugge, "Adaptive, multi-parameter battery state estimator with optimized time-weighting factors," *J. Appl. Electrochemistry*, vol. 37, no. 5, pp. 605–616, 2007.

[29] H. Rahimi-Eichi, F. Baronti, and M.-Y. Chow, "Online adaptive parameter identification and state-of-charge coestimation for lithium-polymer battery cells," *IEEE Trans. Ind. Electron.*, vol. 61, no. 4, pp. 2053–2061, Apr. 2013.

[30] J. Li and M. Liu, "State-of-charge estimation of lithium-ion batteries using composite multi-dimensional features and a neural network," *IET Power Electron.*, vol. 12, no. 6, pp. 1470–1478, 2019.

[31] K. Zhu, Y. Wan, C. Li, and X. Luo, "Battery parameter identification using recursive least squares with variable directional forgetting," in *Proc. IEEE 16th Int. Conf. Control Automat.*, 2020, pp. 755–760.

[32] H.-S. Shin and H.-I. Lee, "A new exponential forgetting algorithm for recursive least-squares parameter estimation," 2020, *arXiv:2004.03910*.

[33] S. Yang et al., "A parameter adaptive method for state of charge estimation of lithium-ion batteries with an improved extended kalman filter," *Sci. Rep.*, vol. 11, no. 1, pp. 1–15, 2021.
[34] P. Xu, B. Liu, X. Hu, T. Ouyang, and N. Chen, "State-of-charge estimation for lithium-ion batteries based on fuzzy information granulation and asymmetric gaussian membership function," *IEEE Trans. Ind. Electron.*, vol. 69, no. 7, pp. 6635–6644, Jul. 2021.
[35] B. Sah, P. Kumar, R. Rayudu, S. K. Bose, and K. P. Inala, "Impact of sampling in the operation of vehicle to grid and its mitigation," *IEEE Trans. Ind. Informat.*, vol. 15, no. 7, pp. 3923–3933, Jul. 2018.
[36] B. Sah, P. Kumar, and S. K. Bose, "A fuzzy logic and artificial neural network-based intelligent controller for a vehicle-to-grid system," *IEEE Syst. J.*, 2020.
[37] *Specification of Li-ion Polymer Battery 3.7 V 10000 mAh, PL-9059156*, AA Portable Power Corp, PL-90591562011, edition 2.0. [Online]. Available: https://www.batteryspace.com/prod-specs/3.7V9059156.pdf
[38] *Product Specification, Rechargeable Lithium Ion Battery, Model: INR18650 M36 T 12.50 Wh*, LG Chem, 2017, rev. 1. [Online]. Available: https://www.nkon.nl/sk/k/m36.pdf
[39] "Product Specification, Rechargeable Lithium Ion Battery," Model: INR18650HG2 3000mAh, LG Chem, 2015, rev. 0. [Online]. Available: https://www.batteryspace.com/prod-specs/9989.specs.pdf

Bikash Sah (Graduate Student Member, IEEE) Bikash received the B.Tech. degree in electrical and electronics engineering from the National Institute of Technology Arunachal Pradesh, Jote, India, in 2014, and the Ph.D. degree in electronics and electrical engineering, specializing in Power and Control, with a thesis titled: An Intelligent Electric Vehicle Charging Infrastructure from the Department of Electronics and Electrical Engineering, Indian Institute of Technology Guwahati, Guwahati, India, in 2021.

He is currently working as Scientific Staff with Bonn-Rhein-Sieg, University of Applied Sciences, Sankt Augustin, Germany. He is also associated with Fraunhofer Institute for Energy Economics and Energy System Technology (Fraunhofer IEE), Kassel, Germany, with a work access contract. His current research interests include vehicle-to-grid systems, electric vehicles and their charging infrastructure, and converter design using wide bandgap devices for renewable energy systems and electric mobility applications.

Dr. Sah was a recipient of the Outstanding Ph.D. Thesis Award by the IEEE Industrial Electronics Society Annual On-Line Conference (ONCON) 2022. He is an active reviewer of many journals such as IEEE TRANSACTIONS ON POWER ELECTRONICS, IEEE ACCESS, IEEE JOURNAL OF EMERGING AND SELECTED TOPICS IN INDUSTRIAL ELECTRONICS, IEEE TRANSACTIONS ON SMART GRIDS, and IEEE OPEN JOURNAL OF THE INDUSTRIAL ELECTRONICS SOCIETY.

Praveen Kumar (Senior Member, IEEE) received the B.Tech. degree in electrical engineering from the National Institute of Technology, Hamirpur, India, in 1998, the M.Tech. degree in energy system from the Indian Institute of Technology Delhi, Delhi, India, in 2000, and the Ph.D. degree in electrical machines from the Delft University of Technology, Delft, The Netherlands, in 2008.

He is currently a Professor with the Indian Institute of Technology Guwahati, Guwahati, India. Prior, he was a Team Leader of Hybrid Systems with Drive Trains Innovation, Eindhoven, The Netherlands, and Cofounder and Chief Technical Officer (CTO) of elmoCAD Engineering GmbH, Bochum, Germany. His current research interests include optimizing electrical motors and drives, hybrid and electric vehicles, smart grid, wired charging, and wireless charging of electric vehicles.

Dr. Kumar is an active reviewer of many journals, including IEEE TRANSACTIONS ON INDUSTRIAL ELECTRONICS, IEEE TRANSACTIONS ON ENERGY CONVERSION, and IEEE TRANSACTIONS ON MAGNETICS.